Microwave Laboratory
W. W. Hansen Laboratories of Physics
Stanford University
Stanford, California

FOLDOVER IN DIODE-LOADED RESONANT CIRCUITS

By

Robert Edward Tokheim

M. L. Report No. 945

August 1962

ABSTRACT

Experimental investigation of foldover has been made in a medium
frequency series resonant circuit using two back-to-back Varicap diodes.
Foldover of this nature is a phenomenon of some importance in several
practical devices, including bistable switching circuits, the parametron,
the parametric limiter, the parametric amplifier and the harmonic genera-
tor. The purpose of this study was to determine how well such foldover
could be predicted from theory for the series circuit. Theoretical results
were based upon precise measurements of the individual circuit components.
Very good agreement of theory with experiment was obtained, assuming only
the fundamental frequency term in the harmonic balance method of solving
the nonlinear differential equation.

ACKNOWLEDGMENT

TABLE OF CONTENTS

LIST OF FIGURES

CHAPTER I

INTRODUCTION

A. BRIEF DESCRIPTION OF FOLDOVER

The term foldover refers to the bending over of the amplitude-frequency
response curve of a nonlinear resonant system--a phenomenon which is due to
the amplitude dependence of the resonant frequency. A typical example of
foldover to the high frequency side is shown in Fig. 1; Fig. 2 is an example
of foldover to the low frequency side. Note that successively higher
driving source amplitudes lead to greater bending over of the respective
curves; hence the curve eventually becomes triple-valued. The middle branch
of the curve is not observed physically because of its instability.

A so-called "jump" phenomenon results wherever the slope of the
response curve becomes infinite. In general, resonant systems which
contain a nonlinear component exhibit two kinds of "jumps" as indicated
in Fig. 3, and the resulting loop indicated is often called a hysteresis
effect. Typical examples are mechanical systems with nonlinear springs,
electronic circuits with nonlinear inductors, and capacitors.

The present study will be concerned with the behavior of a simple
resonant circuit with a nonlinear capacitor, which is realized by variable
capacitance diodes. The purpose of this study will be to compare foldover
in the resonant circuit as observed experimentally with that determined
theoretically. Theoretical calculations will be based upon experimental
measurements of the individual circuit components.

B. EFFECTS OF FOLDOVER IN PRACTICAL DEVICES

Foldover is a phenomenon of some importance in several devices in-
corporating nonlinear elements. Notable examples are the bistable switch-
ing circuit, parametron, parametric limiter, parametric amplifier, and
the harmonic generator.

- 1 -
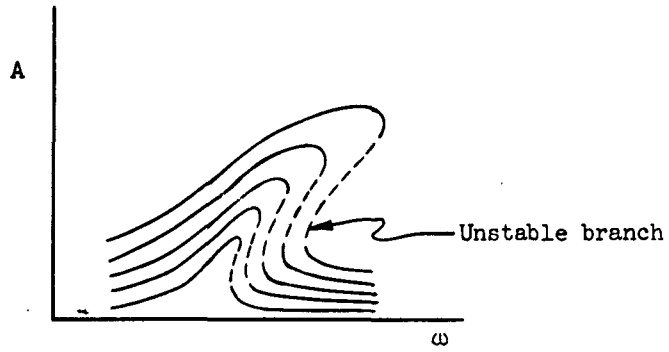
FIG. 1--Foldover to the high frequency side.
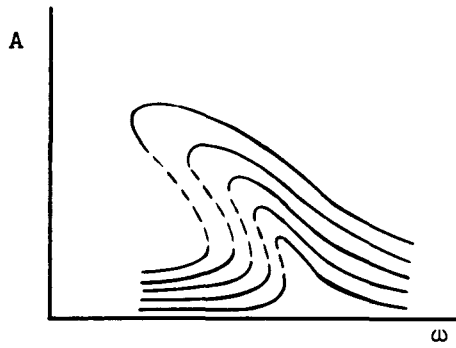
FIG. 2--Foldover to the low frequency side.
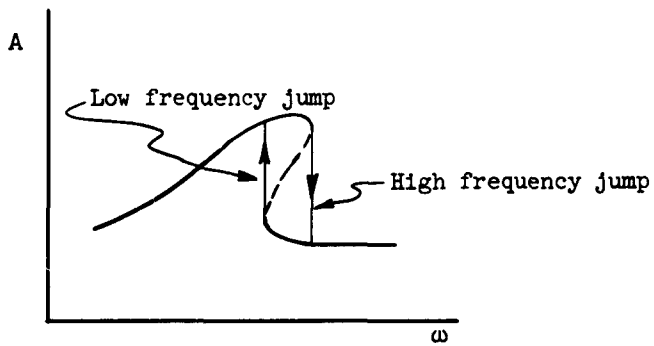
FIG 3--"Jump" phenomenon illustrated.

The bistable switching circuit using a semiconductor abrupt junction diode, which may be utilized in computers, takes two forms. Keizer[1] has described the first kind, which has an rf input and a dc output. The switching action is the aforementioned "jump" behavior at resonance and is controlled by the rectified rf input, which serves as bias for the diode as well as for the dc output. The second kind exhibits essentially the same resonance phenomenon but, since two diodes back-to-back are used, requires no bias and therefore has an rf output.

Both of the above circuits may be contrasted with the parametron, which is also a bistable device useful in computers. The parametron utilizes the two possible phases of the subharmonic output, rather than the output amplitudes, to represent the binary states.

Similar to the parametron are the parametric limiter and the parametric amplifier. All three utilize a nonlinear element which enables transfer of power from the pump frequency to a subharmonic. At large pump levels foldover in the pump circuit can have a significant effect on the performance of the device.

Harmonic generators also exhibit the effects of foldover. DiDomenico et al.,[2] have examined this phenomenon to some degree for their ferroelectric harmonic generator. They showed theoretically and experimentally that the detuning effect of foldover on the input and output circuits accounts in part for output saturation at high power levels.

CHAPTER II

VARIABLE CAPACITANCE DIODES

A. SINGLE DIODE CHARACTERISTIC

In this investigation only the p-n abrupt junction semiconductor diode will be considered. The complete equivalent circuit for such a diode is shown[3] in Fig. 4. The nonlinear junction capacitance is C_s and g , assumed to be linear, represents the conductance of the junction. The series resistance caused by the finite conductivity of the semiconductor material is R_s . The lead inductance is L_o and C_o is the case capacitance, both small quantities. Usually the major loss is due to R_s . In the low and high frequency ranges L_o is negligible. Therefore a useful equivalent circuit becomes the one of Fig. 5, if leakage current is important, or Fig. 6, when dc leakage is not to be considered.

We assume that the external voltage across the diode is

$$V_c = V_{dc} + v \qquad ,$$

where V_{dc} is the static dc bias voltage and v is the dynamic variational voltage (containing both dc and time-varying terms) about the static dc bias, and that the total charge on the diode is

$$Q = Q_{dc} + q \qquad ,$$

where Q_{dc} is the dc charge due to the static bias voltage and q is the variational charge (containing both dc and time-varying terms) about this value.

The variational capacitance is then

$$C(V_c) = \frac{dq}{dv} = \frac{dQ}{dV_c} = C_o + C_1 (V_c + V_o)^{-1/2} \qquad , \qquad (2.1)$$
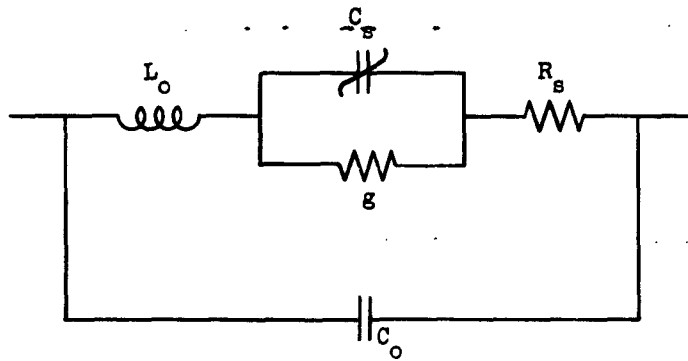
FIG. 4--Encased diode equivalent circuit.
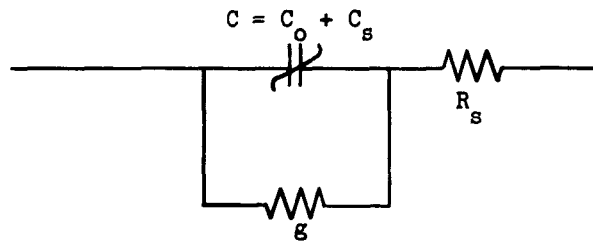
FIG. 5--Approximate diode equivalent circuit.
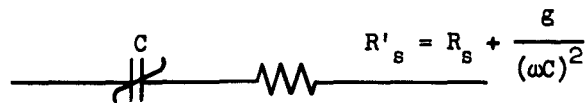
FIG. 6--Equivalent circuit to Fig. 5 for $g \ll \omega C$.

where V_o is the junction contact potential and C_o is the case capacitance. The variational capacitance $C(V_c)$ is sketched in Fig. 7. When $v \ll V_{dc}$ and V_o, the variational capacitance becomes the small signal capacitance

$$C(V_{dc}) = C_o + C_1 (V_{dc} + V_o)^{-1/2} \quad , \qquad (2.2)$$

which is a function of the static dc bias only. At large signal levels the variational capacitance becomes, in addition, a function of v.

In the subsequent analysis of nonlinear resonance it is necessary to have an expression for the variational voltage v across the diode in terms of the variational charge q. This is found by first integrating (2.1),

$$Q = \int_c^{V_c} C(V_c)dV_c = C_o V_c + 2C_1 \left[(V_c + V_o)^{1/2} - V_o^{1/2} \right] \quad . \qquad (2.3)$$

The inverse characteristic (sketched in Fig. 8) is then approximated by a power series in Q retaining only the first three terms:

$$V_c = aQ + bQ^2 + dQ^3 \quad . \qquad (2.4)$$

The desired relation $v(q)$ is then found by substituting $V_c = V_{dc} + v$ and $Q = Q_{dc} + q$ into (2.4). This gives

$$v = a'q + b'q^2 + d'q^3 \quad , \qquad (2.5)$$

where

$$a' = a + 2bQ_{dc} + 3d Q_{dc}^2$$

$$b' = b + 3d Q_{dc}$$

$$d' = d \quad \bullet$$

$$C = C_o + C_1(V_c + V_o)^{-1/2}$$
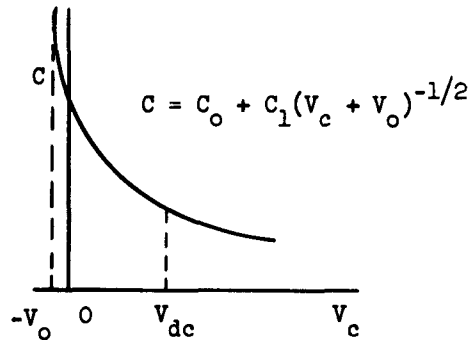
FIG. 7--Single diode capacitance-voltage relationship.
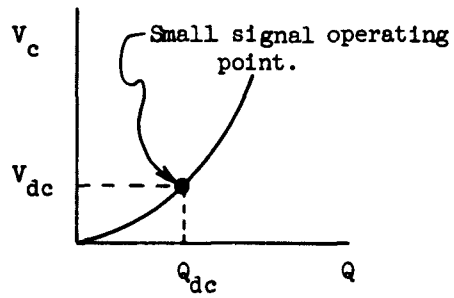
FIG. 8--Single diode voltage-charge curve.

Note that the variational elastance of the single diode as a function of Q is found by differentiating (2.4) with respect to Q :

$$\frac{1}{C} = a + 2bQ + 3dQ^2 \quad .$$
(2.6)

B. BACK-TO-BACK DIODE CHARACTERISTIC

Here we consider two identical abrupt junction semiconductor diodes connected back-to-back. We shall call this unit the back-to-back diode, and for the purposes of this analysis we shall assume that the cathodes are in common.

To investigate the performance of the back-to-back diode, assume that a sinusoidal voltage source is applied across its terminals. Initially both diodes are assumed to conduct in the forward direction until each achieves its maximum charge during the cycle. This net positive charge which is now between the diodes may not escape except by leakage through the high inverse diode resistance on either side. The entrapped charge merely alternates between the two diode cathodes. To examine this in detail, consider Fig. 9. Symbolically, two capacitors are shown, but recall that, as a diode, each conducts in the direction indicated by the arrow. The sinusiodal voltage applied to the diode is v , and Q_1 and Q_2 are the charges on diodes ① and ②, respectively.

When v reaches its positive maximum, the total voltage is across diode ①, and the corresponding maximum charge is Q_0 , or $Q_1 = Q_0$; also $Q_2 = 0$ on diode ②. At the negative maximum of v , we have $Q_2 = Q_0$ and $Q_1 = 0$. Thus the charge Q_0 alternates between the two diodes such that

$$Q_0 = Q_1 + Q_2 \quad .$$
(2.7)

Since the diodes are identical, at $v = 0$ we must have $Q_1 = Q_2 = \frac{Q_0}{2}$. This enables us to sketch the approximate variation of Q_1 and Q_2 with reference to v (Fig. 10). Note that Q_1 and Q_2 are not sinusoidal.
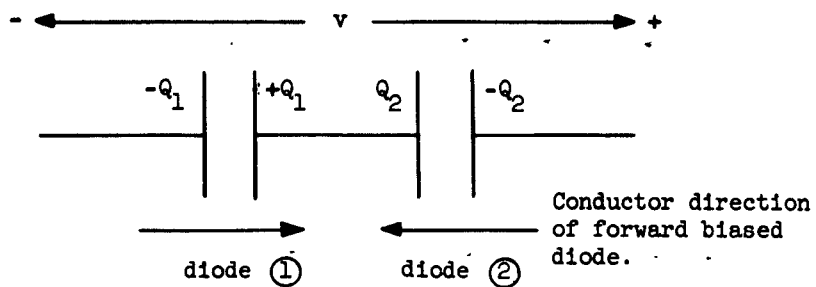
FIG. 9--Capacitive back-to-back diode equivalent circuit.
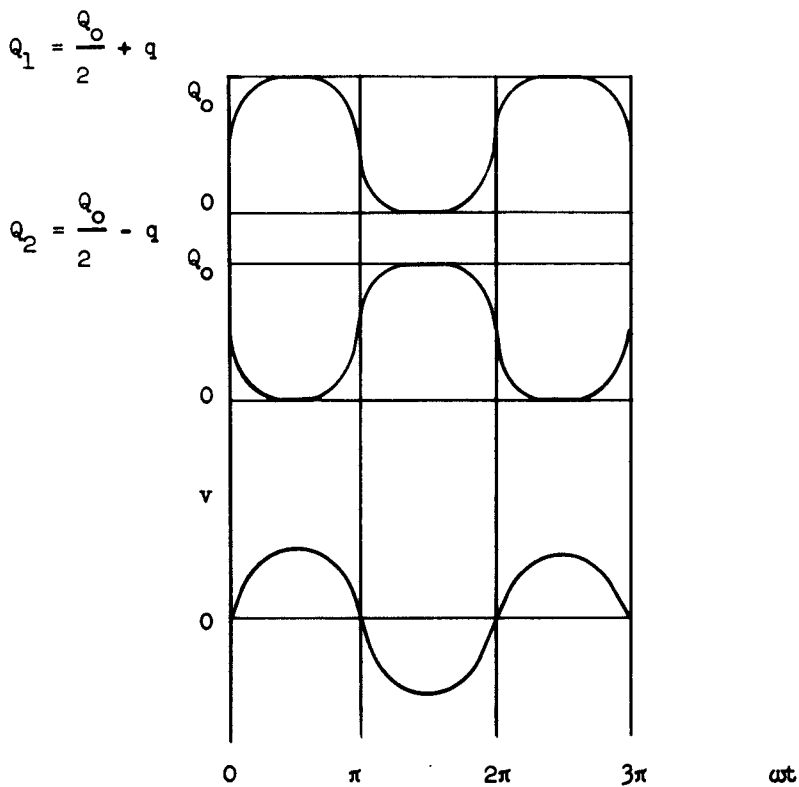
FIG. 10--Steady state back-to-back diode charges and
applied voltage.

Because of the symmetry of the system, the average variational charge on each diode is zero, and therefore

$$< Q_1 > = < Q_2 > = \frac{Q_0}{2} \qquad . \qquad (2.8)$$

The diodes are, then, self-biased to the charge level $Q_0/2$.

With q as the variational charge on each diode and hence in the external circuit, we have

$$q = Q_1 - \frac{Q_0}{2} = \frac{Q_0}{2} - Q_2 \qquad ; \qquad (2.9)$$

therefore

$$\left| q \right| \leq \frac{Q_0}{2} \equiv q_m \qquad . \qquad (2.10)$$

The relation between variational voltage and variational charge is found from

$$v = V_c(q_m + q) - V_c(q_m - q) \qquad , \qquad (2.11)$$

by using the approximation (2.4) to the single diode characteristic $V_c(Q)$. Thus we obtain

$$v = a'q + d'q^3 \qquad , \qquad (2.12)$$

where

$$a' = 2(a + 2bq_m + 3dq_m^2)$$

$$d' = 2d \qquad .$$

Figure 11 shows how v would be constructed graphically directly from $V_c(Q)$, knowing q_m . The variational elastance S of the back-to-back combination is then

$$S = a' + 3d'q^2 \qquad . \qquad (2.13)$$

The back-to-back diode capacitance obtained from (2.13) is sketched in Fig. 12 as a function of q.

- 10 -
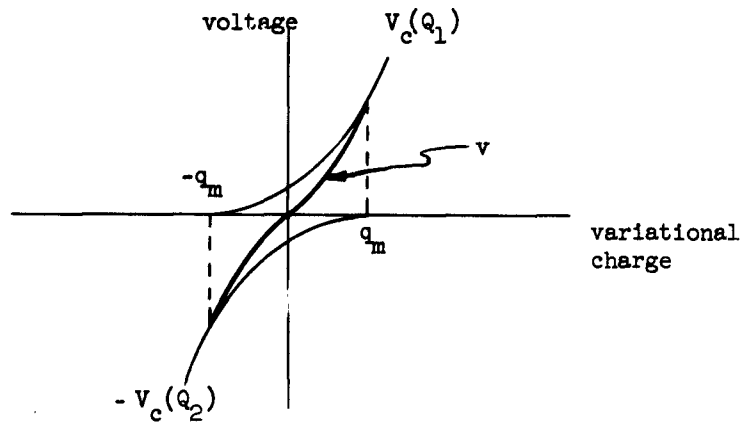
FIG. 11--Construction of back-to-back diode characteristic.
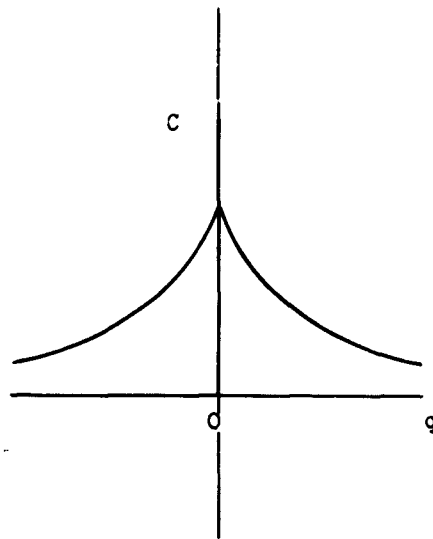
FIG. 12--Back-to-back diode capacitance-charge relationship.

CHAPTER III

THEORETICAL RESONANCE CALCULATIONS

A. SERIES RESONANT CIRCUIT

By considering a lumped element resistance for the losses, we show in Fig. 13 the simple series resonant circuit whose behavior we wish to determine.

In this figure the Thevenin equivalent constant voltage generator V_a has arbitrary but constant phase angle β_o , V_{dc} is the dc bias, L is the ferrite core choke, and the Thevenin equivalent resistance R comprises the inductor, diode, current probe and generator resistances.

B. SOLUTION OF THE BASIC EQUATION

From Fig. 13 we find the series circuit equation to be

$$V_a \cos (\omega t + \beta_o) = R \frac{dq}{dt} + L \frac{d^2 q}{dt^2} + v \quad . \qquad (3.1)$$

For the single diode case the approximation to the diode variational voltage v in terms of the variational charge q is given by (2.5). Thus, we obtain

$$V_a \cos (\omega t + \beta_o) = R \frac{dq}{dt} + L \frac{d^2 q}{dt^2} + a'q + b'q^2 + d'q^3 \quad . \quad (3.2)$$

A trial solution to (3.2) may begin with the linear solution $q = q_m \cos \omega t$. It immediately becomes evident that the quadratic term of (3.2) forces us to assume a dc component of q which varies with q_m^2 . It is this dc component of q which introduces a dependence of the effective bias on the amplitude of the force oscillation. This can lead to the occurrence of relaxation oscillations.
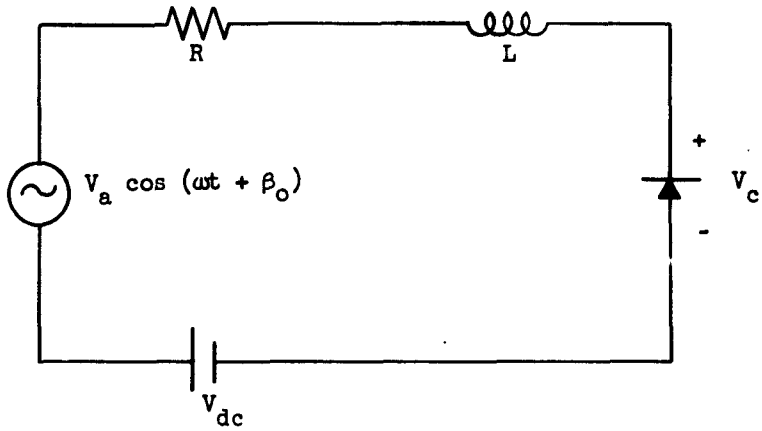
a. Single diode.
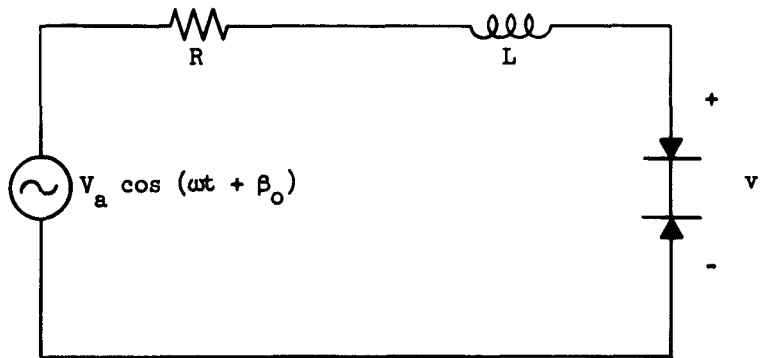
b. Back-to-back diode.

FIG. 13--Series resonant circuit.

For the back-to-back diode case, we insert the diode voltage (2.12) into (3.1), and thus obtain

$$V_a \cos (\omega t + \beta_o) = R \frac{dq}{dt} + L \frac{d^2q}{dt^2} + a'q + d'q^3 \quad . \qquad (3.3)$$

Note that (3.3) contains no quadratic term; since the right hand side of (3.3) is an odd function of q, we see that no dc component will arise in the solution.

Originally we had hoped to avoid relaxation oscillations completely by employing the back-to-back diode. However, since the dynamic bias on the diodes varies with the amplitude of the oscillating charge, it appears that relaxation oscillations may be possible. It has been mentioned already that the back-to-back arrangement requires no external dc bias. Another important advantage of the back-to-back diode is that one obtains greater foldover than with the single diode, since maximum nonlinearity occurs at low signal levels. We should especially note that the back-to-back diode gives foldover to the high frequency side, and the single diode to the low frequency side (Fig. 2). This is predicted by the theory and has been observed experimentally.

We shall now apply the harmonic balance method to the solution of the differential equation (3.3). The procedure is to assume a Fourier series expansion for q and determine the constants by setting the combined coefficients of like frequency terms equal to zero. For our purposes we shall take only the first term of the assumed solution as $q = q_m \cos \omega t$ and substitute it into (3.3). We find immediately the condition on the phase of the source voltage

$$\sin \beta_o = \frac{\omega R q_m}{V_a} \quad . \qquad (3.4)$$

It is useful to speak of the equation error ϵ, obtained by moving the source term to the right hand side of (3.3). This ϵ is a measure of the accuracy of the solution. Thus we have

$$\epsilon = \cos \omega t \left(-V_a \cos \beta_o - L\omega^2 q_m + a' q_m + \frac{3}{4} d' q_m^3 \right)$$

$$+ \cos 3\omega t \left(- \frac{1}{4} d' q_m^3 \right) \quad . \qquad (3.5)$$

- 14 -

In our assumed solution we have only two variables, q_m and ω. Hence, we can only set the coefficients of the first harmonic term equal to zero. The equation error would then be given by the third harmonic term. Given another variable (by adding a $\cos 3\omega t$ term) we could then require the third harmonic term to vanish also. There would then, however, be an error term containing the fifth harmonic.

Equating the first term to zero gives, accordingly,

$$-V_a \cos \beta_0 + q_m (a' - L\omega^2) + \frac{3}{4} d' q_m^3 = 0 \quad . \qquad (3.6)$$

By eliminating β_0 from (3.4) and (3.6), we find

$$V_a^2 = \omega^2 q_m^2 R^2 + [(a' - L\omega^2) q_m + \frac{3}{4} d' q_m^3]^2 \quad . \qquad (3.7)$$

To find $\omega^2(q_m)$ from (3.7), we solve for ω^2:

$$\omega^2 = B \pm (B^2 - C)^{1/2} \quad , \qquad (3.8)$$

where

$$B = \frac{U}{q_m L} - \frac{1}{2} \left(\frac{R}{L}\right)^2 \qquad (3.9)$$

$$C = \left(\frac{U}{q_m L}\right)^2 - \left(\frac{V_a}{q_m L}\right)^2 \quad , \qquad (3.10)$$

and

$$U = a' q_m + \frac{3}{4} d' q_m^3 \quad . \qquad (3.11)$$

It is useful to make further definitions:

$$\alpha = \frac{U}{q_m L} \qquad (3.12)$$

$$\delta = \frac{V_a}{q_m L} \quad , \qquad (3.13)$$

- 15 -

and

$$\gamma = \frac{1}{2}\left|\frac{R}{L}\right|^2 \qquad . \qquad (3.14)$$

By substituting into (3.9) and (3.10) we get

$$B = \alpha - \gamma \qquad (3.15)$$

$$C = \alpha^2 - \delta^2 \qquad . \qquad (3.16)$$

From (3.15), (3.16) and (3.8) we obtain

$$\omega^2 = \alpha - \gamma \pm (\delta^2 - 2\alpha\gamma + \gamma^2)^{1/2} \qquad . \qquad (3.17)$$

Consider the approximation to (3.17), assuming $\gamma \ll \alpha$. This inequality is well satisfied in practice for circuits with reasonably high Q . Equation (3.17) then becomes

$$\omega^2 = \alpha \pm (\delta^2 - 2\alpha\gamma)^{1/2} \qquad . \qquad (3.18)$$

A few comments should perhaps be made about methods of solution other than by harmonic balance.[4] Iteration is one of the most straightforward methods available. Here we assume the linear solution $q_0 = q_m \cos \omega t$ as the zeroth approximation. This solution may be improved by iteration, requiring for each successive approximation that there be no aperiodic terms. This gives an approximation for ω^2 in terms of q_m . The first approximation gives the same result as the harmonic balance method.

Another possible method is that of frequency perturbation. Here we let $\Theta = \omega t$ be the new independent variable and expand q and ω in power series of a perturbation parameter defined as the coefficient of the nonlinear term of the diode variational voltage. We assume periodic boundary conditions and zero initial conditions for all but the zeroth order solution. The result is again the same as above for the first order approximation.

The method of Rauscher which expands about the backbone curve is also an interesting possibility. However, the integrals and results in each

approximation are less amenable to convenient manipulation than are those
of the above methods.

C. FOLDOVER CURVES

The practical procedure we have followed has been to plot the loss-
less response obtained by letting $\gamma = 0$ in (3.18). We obtain

$$\omega^2 = \alpha \pm \delta \qquad \qquad (3.19)$$

In general, unless the loss is excessive, (3.19) gives an excellent
approximation to the actual response curve except in the vicinity of the
resonance peak, where (3.18) should be used. We see that α determines
the backbone, or free oscillation $(V_a = 0)$ curve, and δ, the deviation
of ω^2 about the backbone.

For a circuit with reasonably high Q (i.e., $\gamma \ll \alpha$), the high
frequency jump point (or point of vertical tangency on the high frequency
side) is very nearly on the backbone curve. Therefore we shall calculate
the amplitude of each resonance peak on the backbone curve and then assume
that it corresponds with the point of vertical tangency. Hence, by setting
$\omega^2 = \alpha$, we obtain, from (3.18)

$$\delta^2 = 2\alpha\gamma \qquad \qquad (3.20)$$

as the approximate condition.

The condition on q_m for the low frequency jump point (or point of
vertical tangency on the low frequency side) is found approximately by
differentiating (3.19) with respect to q_m and setting the result to
zero. This gives us

$$4b\, q_m^2 + 7.5d\, q_m^3 = V_a \qquad \qquad (3.21)$$

The reason we may use the lossless response (3.19) to obtain (3.21) is
that the small amplitude associated with the low frequency jump makes
$\delta^2 \gg 2\alpha\gamma$ in (3.18).

CHAPTER IV

EXPERIMENTAL RESULTS

A. CIRCUIT DESCRIPTION

The general circuit arrangement employed to obtain the experimental results is shown in Fig. 14. The selection of components begins with consideration of the nonlinear element, namely, the specifications of the variable capacitance diode. High Q , high maximum working voltage, and a large maximum-to-minimum capacitance ratio are all important factors. Desirable inductor features are high Q and a high self-resonant frequency in comparison with the operating frequency. The Miller 2.5 mh ferrite core rf choke fulfilled these requirements the most satisfactorily. The capacitance of the variable capacitance diodes available then extablishes the resonant frequency of the inductor-capacitor combination to be of the order of 1 Mc. The above, together with knowledge of the frequency ranges of the only low frequency signal generator immediately available, enabled us to select the component values. We found that the series circuit with two 2.5 mh rf chokes in parallel, and with a diode obtained by placing two Pacific Semiconductor V-100 Varicap diodes back-to-back, gave significant foldover within the lowest frequency range (0.35 to 0.75 Mc) of the signal generator.

The signal generator used in this experiment has an output impedance of about 50Ω. Since this series resistance would cause an excessive reduction of the circuit Q , a 10Ω shunt resistor is used to reduce the generator output resistance to a small fraction of the inductor resistance. The circuit current was measured by means of a Tektronix p 6016 current probe and amplifier. The probe behaves much like a transformer, the primary winding of which is the circuit lead itself. Several turns were employed, with almost negligible loading of the series circuit by the probe. The probe output amplifier was followed by the vacuum tube volt-meter (VTVM), which actually monitored the circuit current.
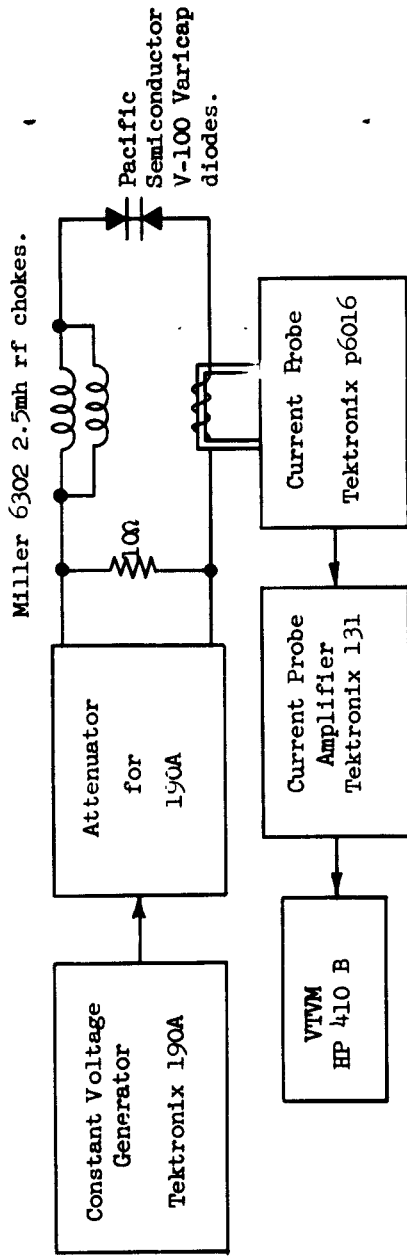
FIG. 14--Circuit arrangement used to obtain experimental results.

B. CALIBRATION OF MEASURING EQUIPMENT

The specifications of the VTVM indicate a flat frequency response over the region of interest and a voltage precision of at least ± 3% full scale. These specifications were checked by various methods, including using a calibrated oscilloscope. By using the VTVM to calibrate the constant voltage generator from 0.35 to 0.75 Mc, we found that the generator voltage decreased at a rate of 2%/Mc with reference to the voltage at 0.45 Mc, the signal resonance frequency of the circuit being studied.

We next used the VTVM to calibrate the current probe gain over the same frequency range, and found that the gain decreased at a rate of 21%/Mc with reference to the gain at 0.45 Mc. The gain is a function of the number of amp-turns on the primary winding of the probe. The number of primary turns was chosen to be $n = 7$ because this gives a safe maximum gain without saturation, even with the maximum circuit current we expect. With $n = 7$ the input impedance of the current probe at 0.75 Mc is a maximum of $3 + j4\Omega$ and at 0.35 Mc, a minimum of $2 + j3\Omega$. These values were calculated from the probe circuit given in the instruction manual. The reactance term in either case has a negligible effect on the resonant frequency. We shall assume, however, an average contribution of 2.5Ω to the series circuit resistance over the entire frequency range.

C. LUMPED CIRCUIT COMPONENTS

The inductance L and the effective resistance R_L of the two 2.5 mh rf chokes in parallel were measured as a function of frequency by the Boonton 160-A R-X meter. Figure 15 shows a plot of the results. Note that the inductance is nearly constant, whereas the resistance more than quadruples from 0.35 to 0.75 Mc. These changes must, of course, be taken into account when calculating foldover curves from theory.

The setup shown in Fig. 16 was used to determine the single diode capacitance as a function of bias voltage V_{dc}. A back-to-back diode combination was used as in the large signal experiment to enable us to test the symmetry of the diodes, which can be done by merely reversing the bias field. The source voltage is made sufficiently small to assure us of measuring only the small signal capacitance, provided that for small
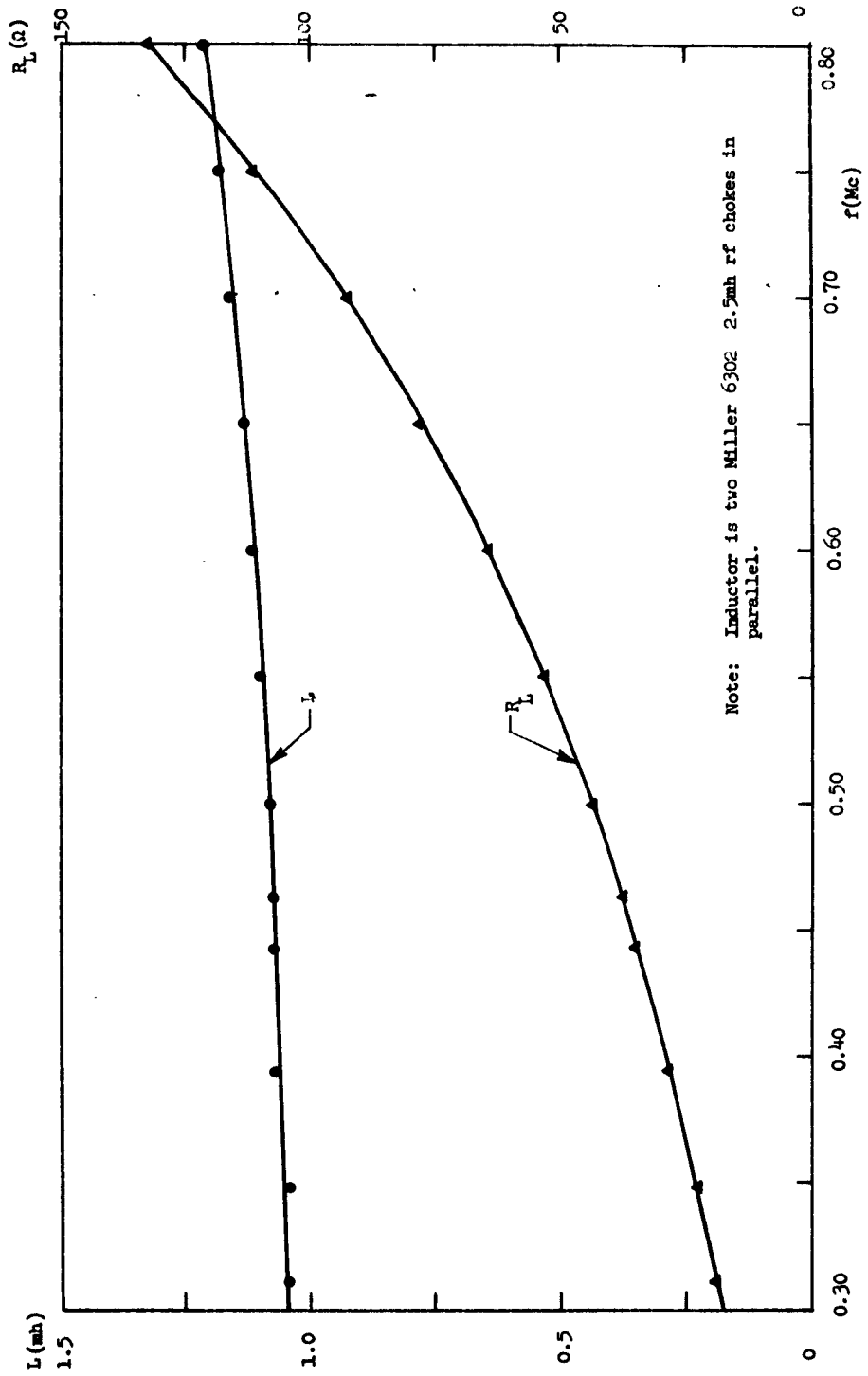
FIG. 15--Measured L and R_L vs. frequency.

Note: Inductor is two Miller 6302 2.5mh rf chokes in parallel.

- 21 -
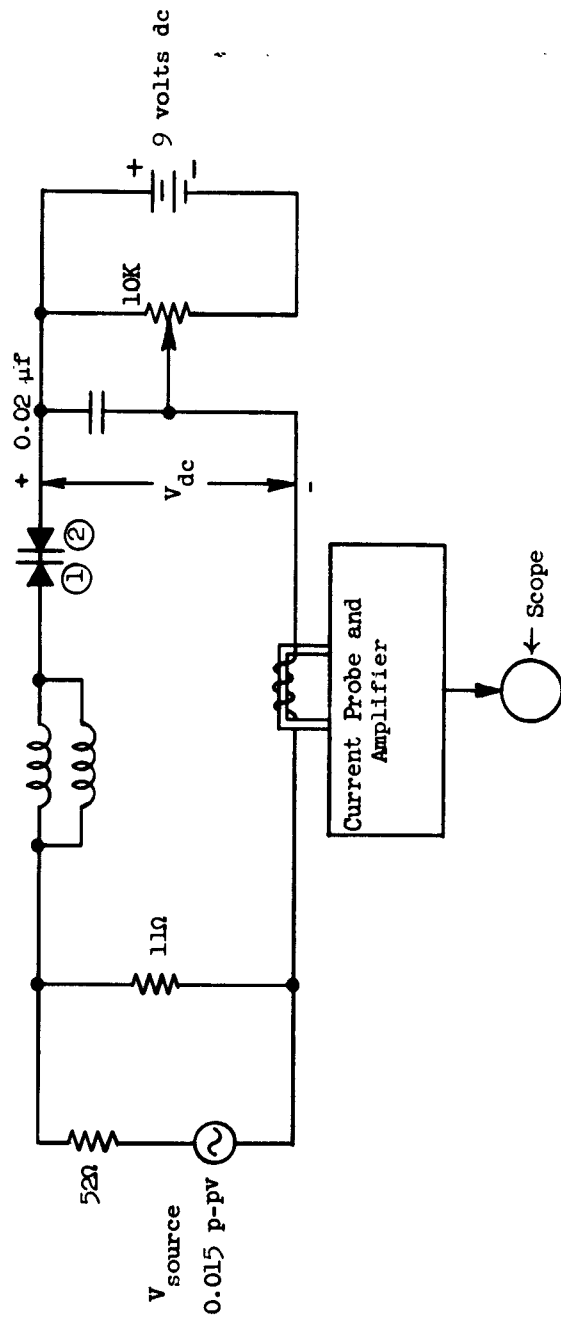
FIG. 16--Circuit used to determine single diode capacitance.

bias voltages, where the capacitance nonlinearity is large, we determine the resonant frequency by extrapolating the small foldover of the current amplitude response to zero.

Consider now, using the same nomenclature as in Chapter II.B, the voltage across the back-to-back diode:

$$v + V_{dc} = V_c(Q_{dc} + \frac{Q_o}{2} + q) - V_c(\frac{Q_o}{2} - q) \qquad , \qquad (4.1)$$

where Q_{dc} is the additional charge on diode ① (Fig. 16) due to V_{dc}. Differentiating with respect to the variational charge q gives the measured elastance

$$\frac{1}{C_m} = \frac{dv}{dq} = \frac{dV_c}{dq}(Q_{dc} + \frac{Q_o}{2} + q) + \frac{dV_c}{dq}(\frac{Q_o}{2} - q) \qquad . \qquad (4.2)$$

Since the external bias does not appear across diode ②, we conclude that for small q, corresponding to the small signal voltage source,

$$\frac{dV_c}{dq}(\frac{Q_o}{2} - q) = \frac{1}{C_{max}} \qquad , \qquad (4.3)$$

where C_{max} is the zero bias single diode capacitance. When $V_{dc} = 0$ we conclude from (4.2) that

$$\frac{1}{C_m(0)} = \frac{dv}{dq} = \frac{2}{C_{max}} \qquad , \qquad (4.4)$$

and we find the single diode capacitance C at a bias voltage V_{dc} by subtracting $1/C_{max}$ from the measured elastance:

$$\frac{1}{C} = \frac{1}{C_m} - \frac{1}{C_{max}} \qquad . \qquad (4.5)$$

From (4.4) and (4.5) we obtain

$$C(V_c) = \frac{2 C_m(0) C_m}{2 C_m(0) - C_m} \qquad . \qquad (4.6)$$

Applying (4.6) to our measurements gives the results plotted in Fig. 17. Note that at 4 volts dc we have $C = 90.6$ μμf , which is well within the ± 20% tolerance on the value 100 μμf specified by the manufacturer.

The best approximate analytical expression to the curve is next determined by assuming the theoretical square root law behavior of the abrupt junction diode (2.1). A good fit was obtained with the expression

$$C = 6.5 + \frac{181}{\sqrt{V_c + 0.6}} \text{μμf} \qquad , \qquad (4.7)$$

giving 0.6 volts as the contact potential and 6.5 μμf as the case capacitance (Fig. 17).

By evaluating the integrated expression for Q , Eq. (2.3), we obtain

$$Q = 0.0065 \, V_c + 0.362 \left[(V_c + 0.6)^{\frac{1}{2}} - 0.78 \right] \qquad , \qquad (4.8)$$

where Q is in units of 10^{-9} coulombs, and will remain so hereafter. We now wish to find $V_c(Q)$ by obtaining the inverse of (4.8). Then we shall determine the back-to-back diode voltage $v(q)$ by the substitution of $V_c(Q)$ into (2.11). If we take the exact inverse of (4.8), the expression we finally get for $v(q)$ is very complicated and makes the differential equation nearly impossible to solve. Therefore, we find the best three-term power series approximation to $V_c(Q)$, the inverse of (4.8), which is plotted in Fig. 18. The resulting approximate expression is

$$V_c = 4.17Q + 6.81 \, Q^2 - 0.44 \, Q^3 \qquad . \qquad (4.9)$$

Equation (2.12) gives the back-to-back diode voltage $v(q)$ in terms of the coefficients of the power series of (4.9). We shall subsequently work with these coefficients (a,b,d) rather than with the voltage expressions themselves.

The last lumped circuit parameter to be considered is the total resistance of the circuit. Figure 15 gives us the effective resistance R_L of the inductor as a function of frequency. From the specification

Pacific Semiconductor V-100 Varicap diode.

● = Experimental points approximate the expression:

$$C = 6.5 + \frac{181}{\sqrt{V_c + 0.6}} \text{ μμf}$$

with $V_c = V_{dc}$

Manufacturer's tolerance

V_{dc} (volts)

$C(\mu\mu f)$
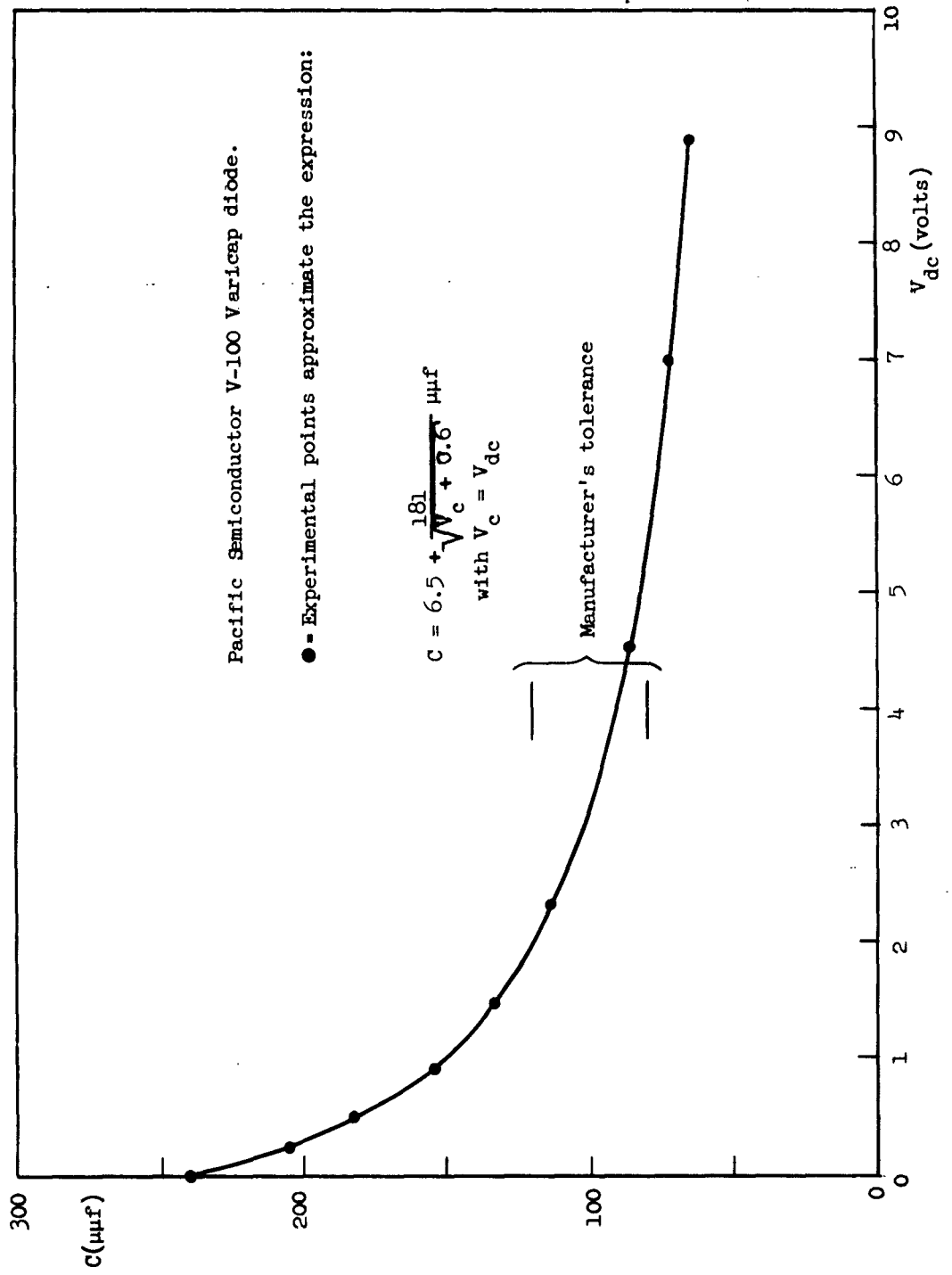
FIG. 17--C vs V_{dc} for single diode.

V_c(volts)

Curve is obtained from inverse of $Q(V_c) = \int_o^{V_c} C(V_c)dV_c$

● Points calculated from the approximate expression:

$V = 4.17Q + 6.81Q^2 - 0.44Q^3$

$Q(10^{-9}$ coulombs)
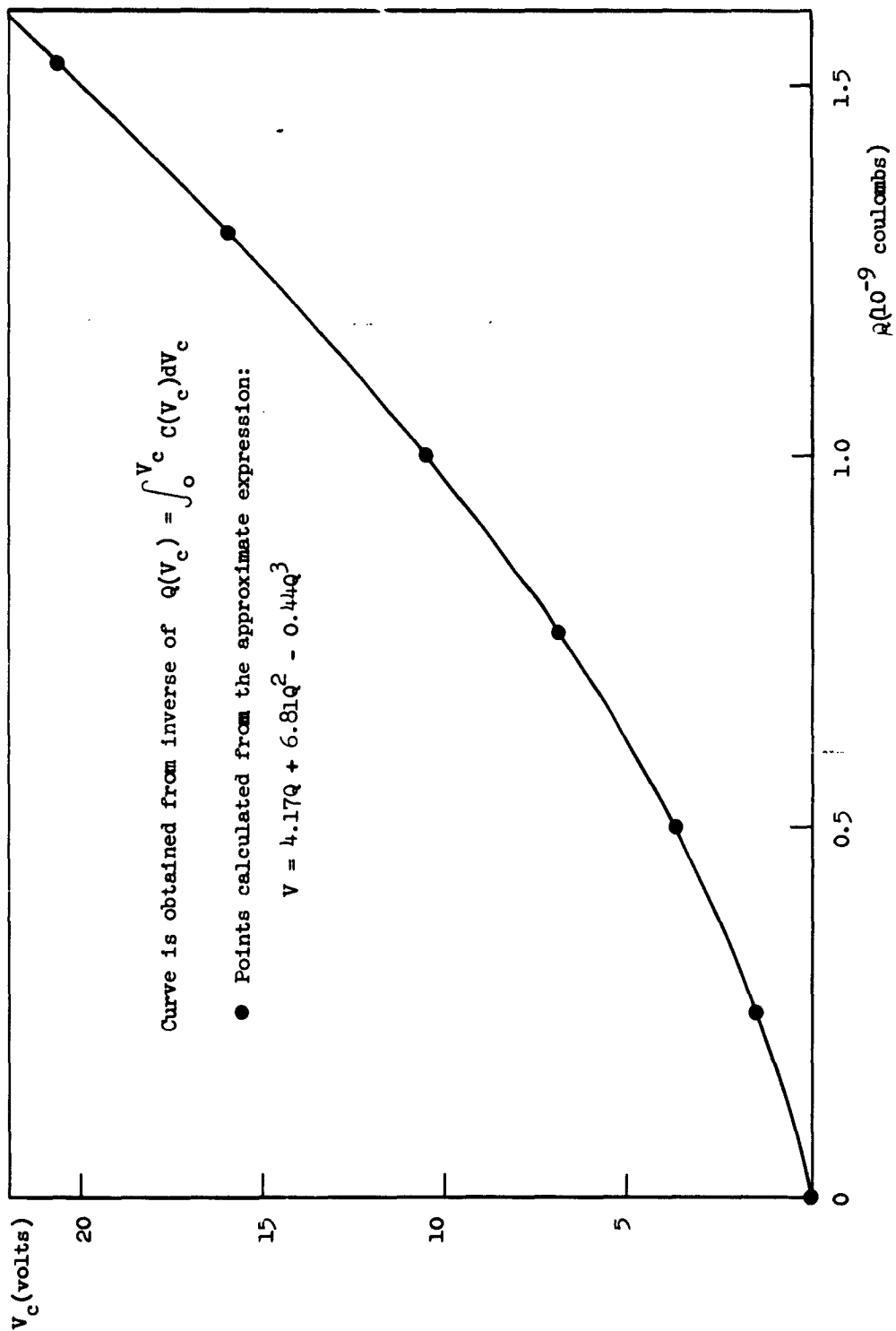
FIG. 18--V_c vs Q for single diode.

sheet for the single diode, we find that $Q = 1600$ at 0.5 Mc. By using the equivalent circuit of Fig. 6, this yields a series resistance R_s' of 2Ω . Hence for the back-to-back diode we get about 4Ω , since the diodes are in series and neither one is conducting. Including the voltage source and current probe resistances, we obtain, then, for the total equivalent resistance of the circuit

$$R = R_L + 14.5\Omega \qquad \qquad (4.10)$$

D. COMPARISON OF EXPERIMENTAL AND THEORETICAL RESULTS

Having determined the lumped components R and L and the $v(q)$ approximation to the back-to-back diode characteristic, we may now calculate the theoretical foldover curves utilizing the simplified equations of Chapter III. The expression for α , Eq. (3.12), is first written in a more useful form,

$$\alpha = \frac{2}{L} (a + 2bq_m + 3.75\, dq_m^2) \qquad \qquad , \quad (4.11)$$

where a , b and d are given by (4.9). Note that the reciprocal of the quantity in brackets in (4.11) is very nearly the single diode elastance (2.6) at $Q = q_m$, the back-to-back diode operating point. This observation suggests that when the approximation to $V_c(Q)$ is found, we should match the slope of V_c rather than the magnitude, if we must make a choice. In the present case both magnitude and slope can be matched. The expressions for δ (3.13) and γ (3.14) are already in simplified form. In order to compare theory with experiment, it is desirable to express amplitude in terms of charge rather than current, that is,

$$I = \dot{q} = - \omega q_m \sin \omega t \qquad \qquad (4.12)$$

and

$$I_{rms} = \frac{\omega q_m}{\sqrt{2}} \qquad , \quad (4.13)$$

which is the quantity actually measured experimentally. When using the lossless expression for ω^2 , Eq. (3.19), we noted that it was more expedient to solve first for $\omega^2 L$, and then to find the frequency from a plot of $\omega^2 L$ vs frequency. Calculations were begun by assuming a value for q_m , then using (3.19) to find I_{rms} vs frequency. For amplitudes greater than one-half the resonance peak, it was necessary to obtain a correction on δL in (3.19) by considering the corresponding term in the more accurate expression (3.18), in order to account for the effect of resistance on the foldover curve.

The experimental results, obtained by the procedure outlined in Chapter IV. A and IV. B and the theoretical results, calculated in the manner described above, are plotted together in Fig. 19. The entire theoretical curve for maximum excitation $(V_a = 0.40)$ is shown to indicate the shape of the resonance. Note that the middle branch of this curve is unstable because it is between the loci of vertical tangents. Curves for other amplitudes are shown in skeleton form, indicating only their high and low frequency jump points. The resistance is given with each amplitude to show how increasing amplitude of excitation forces a change in the resistance by causing greater foldover.

It is useful to compare theoretical with experimental results for the frequencies at the high and low frequency jump points, since these points indicate the behavior at the extremes of the foldover curve. We find the theoretical frequencies to be within ± 0.8% of the experimental values. Theoretical amplitudes of the high frequency jumps are, on the average, 8.6% lower than experimental amplitudes. On the other hand, theoretical amplitudes of the low frequency jumps are, on the average, 16.4% lower than their respective experimental values. Another useful comparison is the amount of foldover, defined as the frequency shift between the two vertical tangent locus points for a given amplitude curve. The amount of foldover for our theoretical maximum amplitude curve is 0.159 Mc, only 6.6% less than the experimental value of 0.170 Mc. Smaller
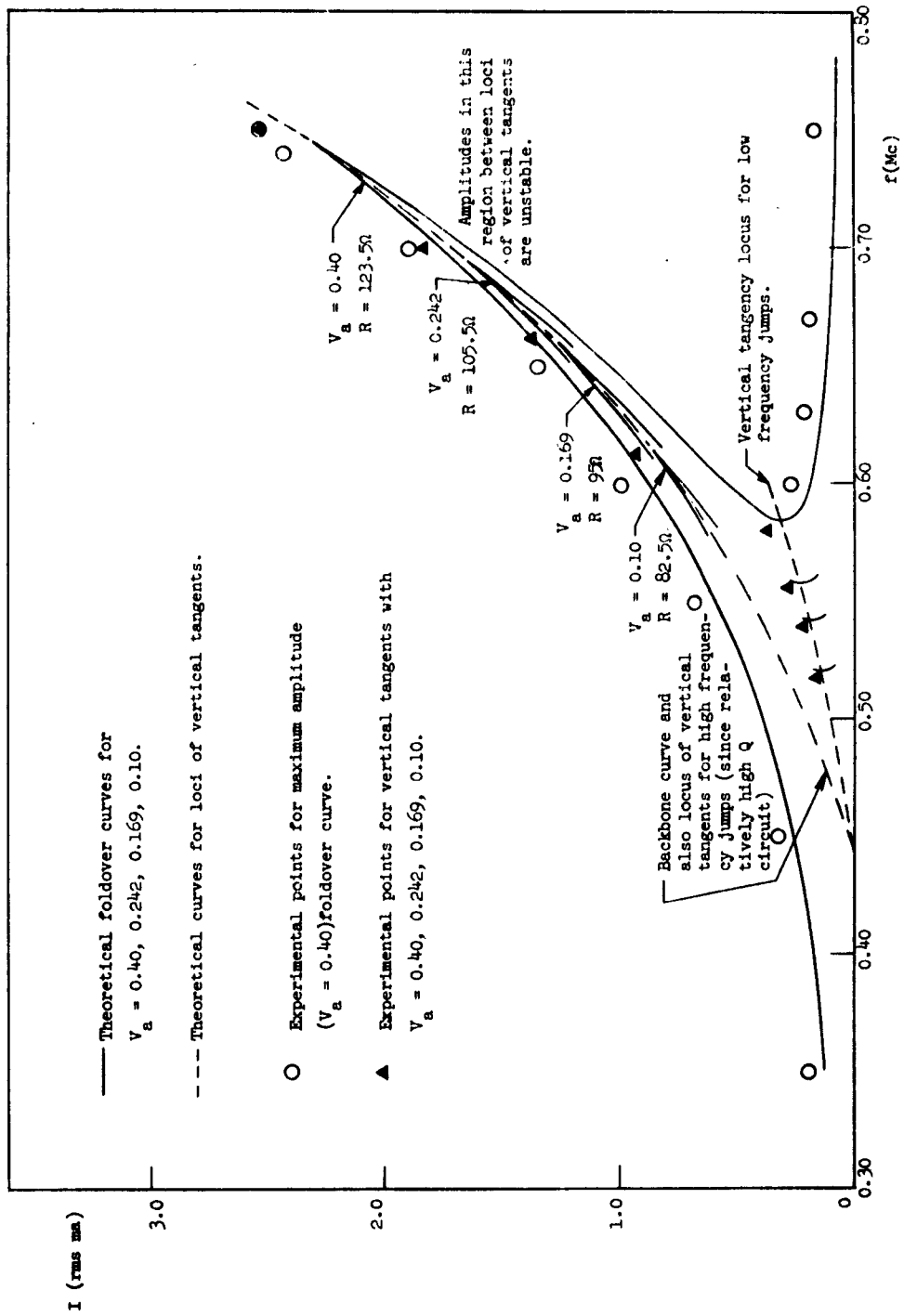
FIG. 19--Series circuit current vs frequency.

I (rms ma)

f(Mc)

Theoretical foldover curves for
V_a = 0.40, 0.242, 0.169, 0.10.

Theoretical curves for loci of vertical tangents.

O   Experimental points for maximum amplitude
(V_a = 0.40)foldover curve.

▲   Experimental points for vertical tangents with
V_a = 0.40, 0.242, 0.169, 0.10.

V_a = 0.40
R = 123.5Ω

V_a = 0.242
R = 105.5Ω

V_a = 0.169
R = 9Ω

V_a = 0.10
R = 82.5Ω

Amplitudes in this
region between loci
of vertical tangents
are unstable.

Vertical tangency locus for low
frequency jumps.

Backbone curve and
also locus of vertical
tangents for high frequen-
cy jumps (since rela-
tively high Q
circuit)

theoretical amplitude curves have a lesser amount of foldover and a corre-spondingly better agreement with the experimental amount of foldover.

The above comparisons indicate very good agreement in frequencies but do not indicate such good agreement in amplitudes. We would find it difficult to account for the difference in amplitudes alone if we considered the effect of component errors on the theoretical results, since the frequencies agree so well. However, the experimental amplitudes themselves may be in error because of the effect of VTVM precision error on V_a and the current probe gain. If this error were present, it could amount to perhaps as much as 10% or so in the amplitude of the foldover curves.

REFERENCES

1. E. O. Keizer, "A Carrier-Energized Bistable Circuit Using Variable-Capacitance Diodes," R.C.A. Review, pp. 475-85, (December, 1957).

2. M. DiDomenico Jr, D.A. Johnson, and R. H. Pantell, "Ferroelectric Harmonic Generator and the Large-Signal Microwave Characteristics of a Ferroelectric Ceramic," J. App. Phys. 33 5, 1697-1706 (May 1962).

3. L. J. Giacoletto, John O'Connel, "A Variable-Capacitance Germanium Junction Diode for UHF," R.C.A. Review, pp. 68-85 (March 1956).

4. J. J. Stoker, Nonlinear Vibrations, Interscience Publishers, Inc., New York, 1950.

DISTRIBUTION LIST
Contract AF 49(638)-415
Project Number 47501

GOVERNMENTAL

Agency	cc	Agency	cc
Commander
AF Research Division
Washington 25, D. C.
Attn: RRRTL	2	Armed Services Technical
Information Agency.	10
		Commander
AF Special Weapons Center
Kirtland Air Force Base
New Mexico
Attn: SWOI	1
Commander
Wright Air Development Division
Wright-Patterson Air Force Base
Ohio
Attn: WWAD	4		
		Director of Research and
Development
Headquarters USAF
Washington 25, D. C.
Attn: AFDRD	1
Commander
AF Cambridge Research Laboratories
Laurence G. Hanscom Field
Bedford, Massachusetts
Attn: CRREL	1		
		Office of Naval Research
Department of the Navy
Washington 25, D. C.
Attn: Code 420	1
Commander
Rome Air Development Center
Griffiss Air Force Base
Rome, New York
Attn: RCOIL-2	1		
		Director, Naval Research Labs.
Washington 25, D. C.
Attn: Technical Information
Officer	1
Commander
Detachment 1
Hq. AF Research Division
The Shell Building
Brussels, Belgium	2		
		Director, Army Research Office
Department of the Army
Washington 25, D. C.
Attn: Scientific Information
Branch	1
P. O. Box AA
Wright-Patterson Air Force Base
Ohio	1		
		Chief, Physics Branch
Division of Research
U. S. Atomic Energy Commission
Washington 25, D. C.	1
Aeronautical Research Laboratories
Building 450
Wright-Patterson Air Force Base
Ohio
Attn: Technical Library	1		
		U. S. Atomic Energy Commission
Technical Information Extension
P. O. Box 62
Oak Ridge, Tennessee	1

- 1 -

Agency	cc	Agency	cc

National Bureau of Standards
Library — 1
Room 203, Northwest Building
Washington 25, D. C.

Director, Department of Commerce — 1
Office of Technical Services
Washington, D. C.

Physics Program — 1
National Science Foundation
Washington 25, D. C.

Director, Office of Ordnance
Research — 1
Box CM, Duke Station
Durham, North Carolina

ARO, Inc. — 1
Arnold Air Force Station
Tullahoma, Tennessee
Attn: AEDC Library

Commanding General — 1
U. S. Army Signal Corps Research
and Development Laboratory
Fort Monmouth, New Jersey
Attn: SIGFM/EL-RPO

Advanced Research Projects Agency — 1
Washington 25, D. C.

Commander — 1
AF Missile Development Center
Holloman Air Force Base
New Mexico
Attn: HDOI

Commander
Army Rocket and Guided Missile
Agency
Redstone Arsenal
Alabama
Attn: ORDXR-OTL

Commandant, Air Force Institute
of Technology (AU) Library — 1
MCLI-LIB, Bldg. 125, Area B
Wright-Patterson Air Force Base
Ohio

Commander — 1
Air Research and Development
Command
Andrews Air Force Base
Washington 25, D. C.
Attn: RDR   2 cys
      RDRA   1 cy
      RDRB   1 cy
      RDRC   1 cy
      RDRS   1 cy

Dr. Bertram A. Mulcahy — 6
Chief, Division of Research
Information
National Aeronautics and Space
Administration
1520 H. Street Northwest
Washington 25, D. C.

Dr. W. R. Luebke — 1
Supporting Research Group
Eitel-McCullough, Inc.
201 Industrial Way
San Carlos, California

General Electric Company — 1
Power Tube Department
Electronic Components Division
Building 269, Room 205
One River Road
Schenectady 5, New York

National Aeronautics and Space
Administration — 6
Washington 25, D. C.

Commander — 1
AF Flight Test Center
Edwards Air Force Base
California
Attn: FTOTL

Chairman — 1
Canadian Joint Staff
For DRB/DSIS
2450 Massachusetts Avenue, N. W.
Washington 25, D. C.

Agency	cc	Agency	cc

Commander
Air Force Cambridge Research
  Laboratories
Office of Aerospace Research
Laurence G. Hanscom Field
Bedford, Massachusetts
Attn· CROOTR   1

Air Force Office of Scientific
  Research   5
Washington 25, D. C.
Attn: SRYP

Office of Naval Research   1
346 Broadway
New York 12, New York
Attn· I. Rowe

Oak Ridge National Laboratory   1
Central Research Laboratory
P. O. Box X
Oak Ridge, Tennessee

Institute for Defense Analysis   1
Research and Engineering Support
  Division
1825 Connecticut Ave., N.W.
Washington 9, D C.
Attn. Technical Information Office

Raytheon Company   1
Research Division
28 Seyon Street
Waltham 54, Massachusetts

Philips Laboratories   1
A Division of North American
  Philips Company, Inc
Irvington-on-Hudson
New York

Wayland D. George   1
Radiation Systems Department
Hughes Aircraft Company
Florence and Teale Streets
Culver City, California

Dr. J. E. Drummond, Head   1
Plasma Physics Laboratory
Boeing Scientific Research Labs.
Boeing Airplane Company
P. O. Box 3707
Seattle 24, Washington

J. W. Nielson, Manager   1
Solid State Materials Lab.
Research Center for the Airtron
  Div. for Litton Industries
200 East Hanover Avenue
Morris Plains, New Jersey

L. F. Broadway, Head   1
Research Laboratories
Electrical and Musical Industries,
  Ltd.
Blyth Road, Hayes
Middlesex, England

H. Okanobori, Chief   1
Planning Section
The Radio Research Labs.
Ministry of Posts and Tele-
  communications
Kokubunji, P. O., Koganei-shi
Tokyo, Japan

General Electric Company   1
Research Laboratory
P. O. Box 1088
Schenectady, New York
Attn: Virgil L. Stout, Manager

Institute of the Aeronautical
  Sciences   1
2 East 64th Street
New York, New York
Attn: Librarian

Dr. J. T. Senise   1
Instituto Technologico de Aero-
  nautica
Sao Jose dos Campos
Sao Paulo, Brazil

Dr. E. Nalos   1
General Electric Research Lab.
European Office
Pelikan Strasse 37
Zurich, Switzerland

SFD Laboratories   1
800 Rahway Avenue
Union, New Jersey
Attn: J. A. Saloom, President

Agency	cc	Agency	cc

W. E. Cantrell — 1
Senior Engineer
Operational and Systems Analysis
Vought Electronics
P. O. Box 1500
Arlington, Texas

Research and Development — 1
Bomac Labs., Inc.
Salem Road
Beverly, Mass.
Attn: Arthur McCoubrey, Manager

Dr. J. C. Anderson — 1
Laboratories RCA, Ltd.
An Associate Company of Radio
    Corporation of America
Zurich 5, Switzerland

Autonetics — 1
A Division of North American
    Aviation, Inc.
9150 E. Imperial Highway
Downey, California
Attn: Technical Librarian

Geophysics Corp. of America — 1
700 Commonwealth Avenue
Boston 15, Mass.
Attn: Dr. H. D. Greyber

Applied Mechanics Reviews — 1
Southwest Research Institute
8500 Culebra Road
San Antonio 6, Texas

Dr. C. W. Barnes — 1
Senior Research Engineer
Electron Devices Lab.
Stanford Research Institute
Menlo Park, Calif.

Radio Research Lab. — 1
Kokubunji P. O.
Tokyo, Japan

Philip S. Carter, Jr.
Stanford Research Institute
333 Ravenswood Avenue
Menlo Park, Calif.

Mr. H. Wilhelmsson — 1
Research Lab. of Electronics
Chalmers Institute of Technology
Gilbraltargatan 5 G
Gothenberg, Sweden

Dr. R. Shersby-Harvie — 1
S.E.R.L.
Baldock, Herts
England

Max-Planck Institute of Physics
    and Astrophysics — 1
Munich, West Germany
(Care of the Librarian)

Dr. J. E. Allen — 1
CNRN Laboratorio Gas Ionizzati
Instituto di Fisica dell'Universita
Piazzale dell Scienze 5
Rome, Italy

The Electronics Department — 1
Royal Institute of Technology
Stockholm, Sweden
(Care of the Librarian)

Dr. Bertil Agdur — 1
Microwave Department
Royal Institute of Technology
Stockholm, Sweden

Professor H. W. Konig — 1
Institut fur Hochfrequenztechnik
Technischen Hochschule
Wien, Austria

Dr. P. J. B. Clarricoats — 1
Dept. of Light Electricl Engr.
The Queen's University
Belfast, Northern Ireland

Stanford Research Institute — 1
Menlo Park, California
Attn: Documents Center

Dr. M. O. Bryand — 1
S.E.R.L. (Admiralty)
West Road, Harlow
Essex, England

Agency	cc	Agency	cc
Dr. J. G. Linhard Euratom Plasma Physics Group Instituto di Fisica dell' Universita Piazzale dell Scienze 5 Rome, Italy	1	Professor R. W. Gould Electron Tube Lab. California Institute of Technology Pasadena, California	1
Christina Walsh Research Lab. of Electronics Chalmers Institute of Technology Gothenberg, Sweden	1	University of Illinois Dept. of Electrical Engr. Urbana, Illinois Attn: P. Coleman	1
CERN Service d'Information Scientifique Geneva 23, Switzerland Attn: Mme. L. Goldschmit-Clermont	1	Columbia University Radiation ab. New York 27, New York Attn: C. Townes	1
The Science Library Science Museum South Kensington London, S. W. England	1	University of Minnesota Electrical Engr. Department Minneapolis 14, Minnesota Attn: H. Oskam	1
Professor Donald C. Stinson Electrical Engineering Dept. University of Arizona Tucson 25, Arizona	1	Northeastern University Physics Department Boston, Mass Attn: G. Lanza	1
University of Southern California Electrical Engr. Dept Los Angeles 7, Calif. Attn Z. Kaprielian	1	Stevens Institute of Technology Physics Dept. Hoboken, New Jersey Attn: W. Bostick	1
Dr. A L Cullen Dept. of Electrical Engineering University of Sheffield St. George's Square Shieffield 1, England	1	University of New Hampshire Department of Physics Durham, New Hampshire Attn: L. Mower	1
Dr. Hellmut Golde Dept. of Electrical Engineering University of Washington Seattle 5, Washington	1	University of California Electronics Research Lab. Berkeley 4, California Attn: J. Whinnery	1
The University of British Columbia Dept. of Electrical Engineering Microwave Lab. Vancouver 8, British Columbia Canada Attn: Dr. G. B. Walker	1	Professor Elie Roubine 78, Avenue des Ternes-XVII Paris, France Rutgers University Microwave Lab. New Brunswick, New Jersey Attn: M. Sirkis	1 1

Agency	cc

New York University 1
Institute of Math. Sciences
25 Waverly Place
New York 3, New York
Attn: M. Kline

California Inst. of Tech. 1
Electrical Engineering Dept.
Pasadena, California
Attn: C. Papas

Oxford University 1
Oxford, England
Attn: H. Motz

Brooklyn Polytechnic Institute 1
Microwave Research Institute
55 Johnson Street
Brooklyn 1, New York
Attn: N. Marcuvitz

Applied Physics Laboratory 1
The Johns Hopkins University
8621 Georgia Avenue
Silver Springs, Maryland
Attn: Library

Dr. Gunter Ecker 1
Institut fur Theoretische Physik
Universitat
Bonn, West Germany

Professor G. K. Emeleus 1
The Queen's University
Belfast, Northern Ireland

J. Van Bladel 1
University of Wisconsin
Dept. of Electrical Engr.
Madison 6, Wisconsin

Cornell University 1
School of Electrical Engr.
Ithaca, New York
Attn: Professor G. C Dalman